Available online at www.sciencedirect.com
ScienceDirect
Trans. Nonferrous Met. Soc. China 33(2023) 2660−2671
Transactions of Nonferrous Metals Society of China
www.tnmsc.cn

Hot deformation temperature and pre-deformation effect on silicide precipitation behavior of (TiB+Y_2O_3)/near α-Ti matrix composite

Qi-hao LIAN[1], Chang-jiang ZHANG[1,2,3], Hong FENG[1], Zhen-bo YANG[1], Shu-zhi ZHANG[1], Jian-chao HAN[2], Tao WANG[2], Fan PENG[3], Peng CAO[4]

1. College of Materials Science and Engineering, Taiyuan University of Technology, Taiyuan 030024, China;
2. Engineering Research Center of Advanced Metal Composites Forming Technology and Equipment, Ministry of Education, Taiyuan 030024, China;
3. Kocel Machinery Co., Ltd., Yinchuan 750021, China;
4. Department of Chemical and Materials Engineering, University of Auckland, New Zealand

Received 20 March 2022; accepted 10 June 2022

Abstract: Based on the hot compression tests, the effects of deformation temperature and pre-deformation on the microstructure evolution of a hybrid (TiB+Y_2O_3)/near α-Ti matrix composite were studied. The results indicate that the size of silicide precipitated increases with increasing deformation temperature, but its quantity increases first and then decreases. Pre-deformation makes the precipitation position of silicide transform from α/β interfaces or β blocks to uniform distribution inside the matrix. Dynamic recrystallization (DRX) is the main reason for grain refinement of composite, and the dislocations produced by pre-deformation accelerate the process of continuous dynamic recrystallization (CDRX). During the deformation process, dislocations proliferate and aggregate around the broken TiB_w and polymerized Y_2O_3 reinforcements, which promotes the refinement of local grains. Different from the effect of TiB_w and Y_2O_3 on the grain refinement, nano silicides promote the DRX of α grains by pinning grain boundaries and blocking the movement of dislocations according to their different distribution positions.

Key words: near α-Ti matrix composite; microstructure evolution; silicide precipitation; dynamic recrystallization; hot compression deformation

1 Introduction

Titanium matrix composites (TMCs) are regarded as advanced structural materials with important application prospects in cutting-edge technology fields such as aerospace and military equipment because of their high specific strength, high creep resistance and excellent corrosion resistance [1,2]. With the advantages of high elastic modulus and good compatibility with the matrix, TiB and Y_2O_3 are considered high-quality reinforcements for the preparation of TMCs [3]. ZHANG et al [4] reported that TMCs with uniformly distributed micrometer sized TiB_w and submicrometer sized Y_2O_3 particles obtained extremely high ultimate tensile strength (1.47 GPa) at room temperature.

At present, the long-term service temperature of widely used Ti−Al−Sn−Zr−Mo−Si high temperature titanium alloys has reached the thermal barrier temperature (600 °C) [5], such as IMI834 [6], Ti-1100 [7], Ti60 [8] and Ti600 [9]. If the temperature is further increased, its high-temperature strength and oxidation resistance will decline sharply, which seriously limits its application at higher temperatures [10]. Some studies [11,12] have pointed out that the decline of

Corresponding author: Chang-jiang ZHANG, Tel/Fax: +86-351-6010022, E-mail: zhangchangjiang@tyut.edu.cn
DOI: 10.1016/S1003-6326(23)66288-0

thermal strength and plasticity of titanium alloy is closely related to the precipitation of silicides, and the uneven and coarse precipitated silicides do great damage to the properties of alloy. Therefore, reasonable regulation of the shape, size and precipitation position of silicide is the key to further improve the service temperature of high temperature titanium alloy.

As a fast eutectoid element, Si usually exists in high temperature titanium alloy in the form of solid solution in matrix or silicide. The silicides in high temperature titanium alloy are mainly $(Ti,Zr)_5Si_3$ (S1 type) and $(Ti,Zr)_6Si_3$ (S2 type). S1 generally presents a rod or needle shape, while S2 mostly presents a spherical or ellipsoidal shape [13,14]. When heat treatment or thermal deformation occurs in α+β two phase zone or β single phase zone, the content of β phase in titanium alloy matrix is high, which is conducive to the precipitation of silicides. JIA et al [15] conducted aging treatment of Ti60 alloy at 650 to 750 °C for different time, and found that during low temperature aging, the silicides were mainly precipitated in β phase and were not sensitive to aging time. In contrast, with the increase of aging temperature and time, silicides coarsened and began to precipitate in α phase. In $(Ti_5Si_3 + TiB_w)$/Ti6Al4V composite, the size and proportion of silicide increase with the increase of aging temperature. Moreover, because the high temperature increases the diffusion rate of Si, the morphology of silicide changes from needle to ellipsoid [16]. However, previous studies mainly focused on the precipitation behavior of silicide during heat treatment. Different from heat treatment process, hot working deformation can promote the precipitation of silicides, and the dislocations become an important precipitation position [17−19]. Previously, we have observed the dynamic precipitation behavior of silicide during severe plastic deformation of high temperature titanium alloy [20], but its mechanism is not clear, and the dynamic precipitation has not been reported. For $(TiB_w + Y_2O_3)$/near α-Ti matrix composite, which is a higher temperature resistant material, it is more meaningful to study the precipitation behavior of silicide in thermal deformation.

In this study, a novel $(TiB_w+Y_2O_3)$/TMCs was prepared and subjected to isothermal compression at different temperatures. The main purpose of this study is to reveal the effect of deformation temperature and pre-deformation on the precipitation behavior of silicide and the roles of reinforcements on dynamic recrystallization (DRX). Furthermore, the influence of pre-deformation on DRX mechanism is systematically analyzed, and a process design thinking is provided for regulating the uniform and fine precipitation of silicide.

2 Experimental

On the basis of the traditional composition of near α high temperature titanium alloy, the material used in this experiment moderately increased the content of Zr element, and added a certain amount of refractory alloy elements Nb and W. The purpose was to improve the thermal strength and creep properties of the composite. The nominal composition of the matrix alloy was Ti−6.5Al−2.5Sn−9Zr−0.5Mo−1Nb−1W−0.25Si with 2 vol.% TiB_w (formed by in situ reaction between TiB_2 powder and matrix) and 0.5 vol.% Y_2O_3 (obtained by adding Y_2O_3 powder) as reinforcements. The raw materials used in the preparation process were pressed titanium (purity >99 wt.%), high purity aluminum blocks, high purity tin blocks, high purity zirconium blocks and crystalline silicon particles. Mo, Nb and W were refractory metals with high melting points and were added in the form of Al−Mo (Mo 50.5 wt.%), Al−Nb (Nb 52.5 wt.%) and Al−W (W 53.7 wt.%) intermediate alloys. In addition, Al, Sn and Zr elements were easy to burn out in the smelting process, and the compensation amounts of 10 wt.%, 7 wt.% and 8 wt.% were used for compensation respectively. Finally, composite ingot was gained by vacuum induction melting. The β transition temperature of the composite was (970±10) °C by theoretical calculation and quenching metallography.

In order to reduce casting defects and refine the initial β grains, the composite ingot was pre-deformed (isothermal multidirectional free forging) by a four-column hydraulic press in the β-phase region. In the whole forging process, the ingot was deformed three passes (deformation per pass: 50%) along the axial and radial directions, respectively. The deformation temperature was 1070 °C, the strain rate was 0.05 s^{-1}, and was air cooled after forging. Isothermal compression experiments were carried out on composite samples (cylinders: d8 mm × 12 mm) using Gleeble−3800

thermal simulation testing machine. Constant strain rate of 0.01 s^{-1} and three different deformation temperatures of 800, 900 and 1000 °C with a total deformation of 90% were used to carry out isothermal compression on the as-cast and as-forged composite samples respectively. Both ends of the cylindrical samples used for the experiment were mechanically polished and lubricated with graphite sheets to ensure good contact between the sample and the indenter.

The microstructure was characterized by MIRA3 LMH scanning electron microscope (SEM) equipped with energy dispersive X-ray spectrometry (EDS) system and JEM−F200 field emission transmission electron microscope (TEM). The samples used for SEM observation were first mechanically ground on water sandpaper until they were smooth, followed by electrochemical polishing and corrosion. The polishing fluid was composed of 60 vol.% methanol, 30 vol.% *n*-butanol and 10 vol.% perchloric acid, and the corrosion solution was Kroll reagent. In addition, the samples for TEM observation were first cut into round sheets (*d*3 mm × 0.5 mm) and then mechanically ground to about 40 μm. Finally, the RES102 multifunctional ion thinning instrument was used for thinning. The grain size of the composite was measured by Image-Pro Plus 6.0 (IPP) software. The deformation behavior of the composite was analyzed by electron backscatter diffraction (EBSD). The preparation method of the samples was the same as that of SEM, but there was no need for corrosion. The data acquisition was completed by the Quanta 200FEG SEM equipped with EBSD system, and the collected data were post processed by Channel 5.0 software.

3 Results and discussion

3.1 Initial microstructure

Figure 1 shows the micrographs of as-cast and as-forged composite. As shown in Fig. 1(a), the as-cast composite presents a basketweave structure, which is composed of staggered α colony. Inside the α colony, the α lamellas and the β phases are separated and arranged in parallel. The whisker shaped reinforcements with a large aspect ratio are TiB_w and the white particle reinforcements are Y_2O_3. TiB_w clusters are on the surface of α lamellas, and Y_2O_3 particles are randomly distributed in the composite matrix. According to Figs. 1(b) and (c), after forging, the α lamellas were refined and the average thickness of the lamellas was reduced from about 2.52 to 2.15 μm. Y_2O_3 polymerized into large particle groups, and the TiB_w reinforcements with a high aspect ratio were broken into several segments. In addition, the twisting of α lamellas can be observed, which is conducive to the globularization of α lamellas [18].

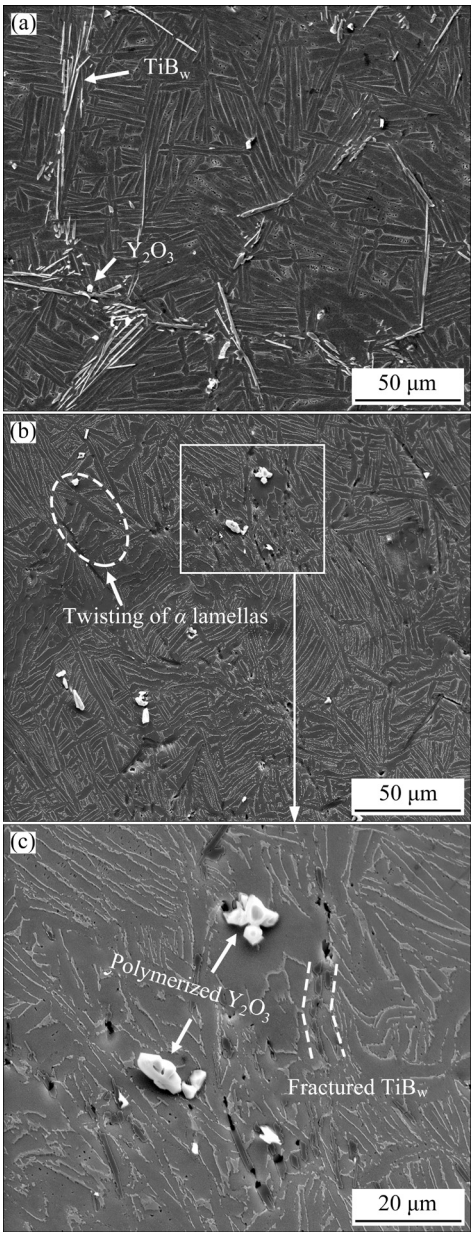

Fig. 1 SEM images of composite: (a) As-cast; (b, c) As-forged

3.2 Microstructure evolution during hot compression

The backscatter electron (BSE) morphology and EDS detection of nano precipitates of as-cast

composite after compression at different temperatures are displayed in Fig. 2. When the thermal compression temperature was 800 °C (Fig. 2(a)), globularization of α lamellas occurred near the fractured TiB_w. Due to the incongruity with the matrix deformation, TiB_w reinforcements were fractured and caused stress concentration, which could promote the subsequent DRX [21]. CHEN et al [22] proved that the fracture of TiB_w reinforcements and equiaxial process of lamellar structure during thermal deformation can effectively improve the strength, plasticity and creep properties of $(TiB_w+(Ti,Zr)_5Si_3)$/TA15 composite. Besides, some nano precipitates were found in the β blocks. In order to determine the phase composition, the microstructure shown in Fig. 2(a) was examined by TEM. According to the selected area electron diffraction (SAED) and EDS results (Figs. 2(d, e)), it can be determined that the precipitate is S2 silicide with a size of about 250 nm. Zr element plays an important role in the precipitation of silicides. Generally speaking, the solid solubility of Si in matrix decreases with the increase of Zr content [23]. The higher Zr content (9 wt.% in this study) and the higher Si content in β phases create favorable conditions for the precipitation of silicides. Therefore, the silicides tend to precipitate in the β blocks through the short-range diffusion of Si element during thermal compression at 800 °C. As shown in Fig. 2(b), the quantity and size of silicide are increased at 900 °C. It may be because higher temperatures improve the element diffusion ability and provide more activation energy for the nucleation of silicides. However, under the deformation condition of 1000 °C (Fig. 2(c)), the amount of precipitated silicide decreases, but the size becomes larger, and the matrix transforms into a full lamellar organization. This indicates that high deformation temperature not only improves the solid solubility of Si, but also increases the matrix flow and dislocation annihilation velocity. The diffusion paths of Zr and Si atoms are reduced, which inhibits the precipitation of silicides. However, the diffusion ability of elements is strong at high temperatures, and Zr and Si atoms can carry out long-range diffusion. Besides, due to the small number of silicides nucleating, it is difficult to form a competitive relationship with each other, resulting in the coarsening of silicides.

Figure 3 shows the microstructure of as-forged composite at different hot compression temperatures. After compression deformation at 800 °C (Fig. 3(a)), the microstructure of the as-forged composite consists of a large number of equiaxed α grains and intergranular residual β phases. These remnant β phases present a water drop shape, which cooperates with silicides and reinforcements to block the growth of spheroidized α grains. As shown in Fig. 3(b), with the increase of deformation temperature, the matrix transforms into duplex microstructure, which is composed of equiaxed α grains and transformed β. Furthermore, the size of silicide also becomes larger. Significantly,

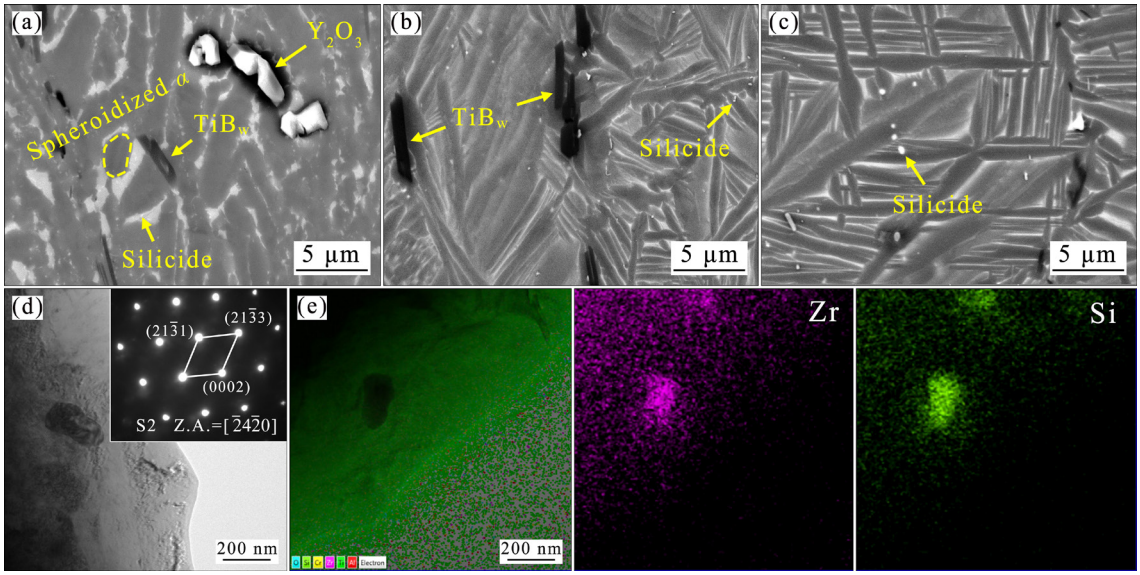

Fig. 2 BSE images of as-cast composite after thermal compression at 800 °C (a), 900 °C (b) and 1000 °C (c), TEM image of precipitate and its corresponding SAED image (d), and EDS face scan results (e)

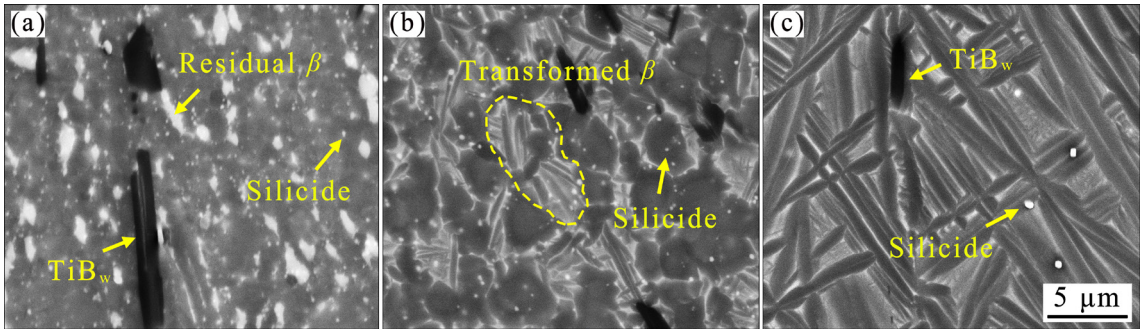

Fig. 3 BSE images of as-forged composite after thermal compression at 800 °C (a), 900 °C (b), and 1000 °C (c)

the silicides of the as-forged samples precipitate uniformly and diffusely on the matrix, not only at the α/β interfaces or β blocks. During the forging process, lots of dislocations accumulate on the composite matrix, especially in the regions of grain boundaries and reinforcements, which can be atomic diffusion channels [17]. Zr and Si atoms diffused rapidly along the channel formed by dislocations and eventually converged inside the grains to precipitate silicides. The dislocations produced by forging are pinned by reinforcements in the subsequent compression process, and high-density dislocations gather around the reinforcements, which promotes the precipitation of silicides. Similar to the as-cast samples, silicides are small in quantity and bulky in size when the as-forged samples deform at 1000 °C (Fig. 3(c)), which is mainly related to the strong diffusion ability of elements at high temperatures but few diffusion paths.

3.3 Flow behavior of composite

The flow stress−strain curves of the as-cast and as-forged composites compressed at different temperatures are shown in Fig. 4. All the flow stress curves show a similar trend, that is, with the increase of strain, the flow stress first increases rapidly until the peak value, then decreases in varying degrees, and finally tends to be stable, which is the result of the joint action of work hardening, dynamic recovery (DRV), DRX and dynamic α globularization (DαG) [18]. As shown in Fig. 4, with increasing deformation temperature, the flow peak stress decreases, the dynamic softening interval shortens, and the dynamic equilibrium interval expands. This is due to the strong migration ability of grain boundaries and dislocations at high temperatures, low dislocation density caused

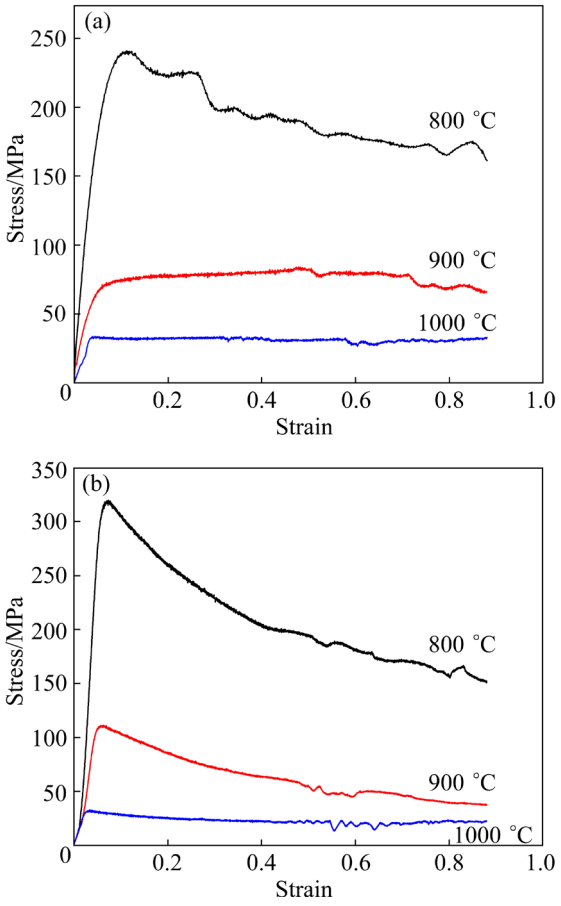

Fig. 4 Stress−strain curves of composite compressed at different temperatures: (a) As-cast; (b) As-forged

by deformation and weak work hardening. In addition, the conversion rate from α phase to β phase increases with the increase of temperature, and the dynamic softening of β phase is easier, so the strain required to reach dynamic equilibrium decreases. Comparing Figs. 4(a) and (b), it can be found that the peak stress of as-forged specimens is remarkably higher than that of as-cast specimens at 800 and 900 °C, while the flow stress curves are almost the same at 1000 °C. At the initial stage of compression, the dislocation density of the

composite increases sharply, and the more dispersed and fine precipitated silicides in as-forged specimens compressed at 800 and 900 °C hinder the movement of dislocations and cause dislocation entanglement. Macroscopically, it shows high work hardening and peak stress. However, after compression at 1000 °C, the two kinds of specimens have similar matrix structure and precipitate distribution, so their flow stress curves are consistent.

3.4 DRX behavior of *α* phase

In order to study the influence of pre-deformation on the DRX mechanism, the corresponding EBSD analysis is put into effect. As shown in Figs. 5(a) and (d), after hot compression at 800 °C, the microstructure of as-cast composite is made up of a large number of coarse substructure or deformed morphology, and new fined grains are formed at the junction of coarse grains. However, the microstructure of as-forged composite is mostly fine equiaxed grains, showing an obvious DRX feature. The grain size of the as-forged samples is significantly finer than that of the as-cast samples, from about 1.23 μm down to 0.89 μm (Figs. 6(a, b)). This is mainly due to the relatively high degree of DRX. In addition, the grain boundary distribution of composite in different initial states can also be obtained from Fig. 5 (high angle grain boundaries (HAGBs) and low angle grain boundaries (LAGBs) are represented by black and white respectively). It can be seen that high-density sub-grain boundaries are accumulated in large-size deformed grains. Through quantitative analysis, the quantity of LAGBs decreased from 24.1% to 14.8% (Figs. 6(c, d)), indicating the transformation from LAGBs to HAGBs during DRX.

According to previous studies, the Kernel Average Misorientation (KAM) map can be used to characterize the strain state and dislocation density of titanium alloy [24]. The lowest and highest KAM values are shown in blue and red respectively. High strain can be observed in the elongated grains in Fig. 5(b), which indicates that a large number of dislocations are stored in the deformed grains due to the lower deformation temperature and higher

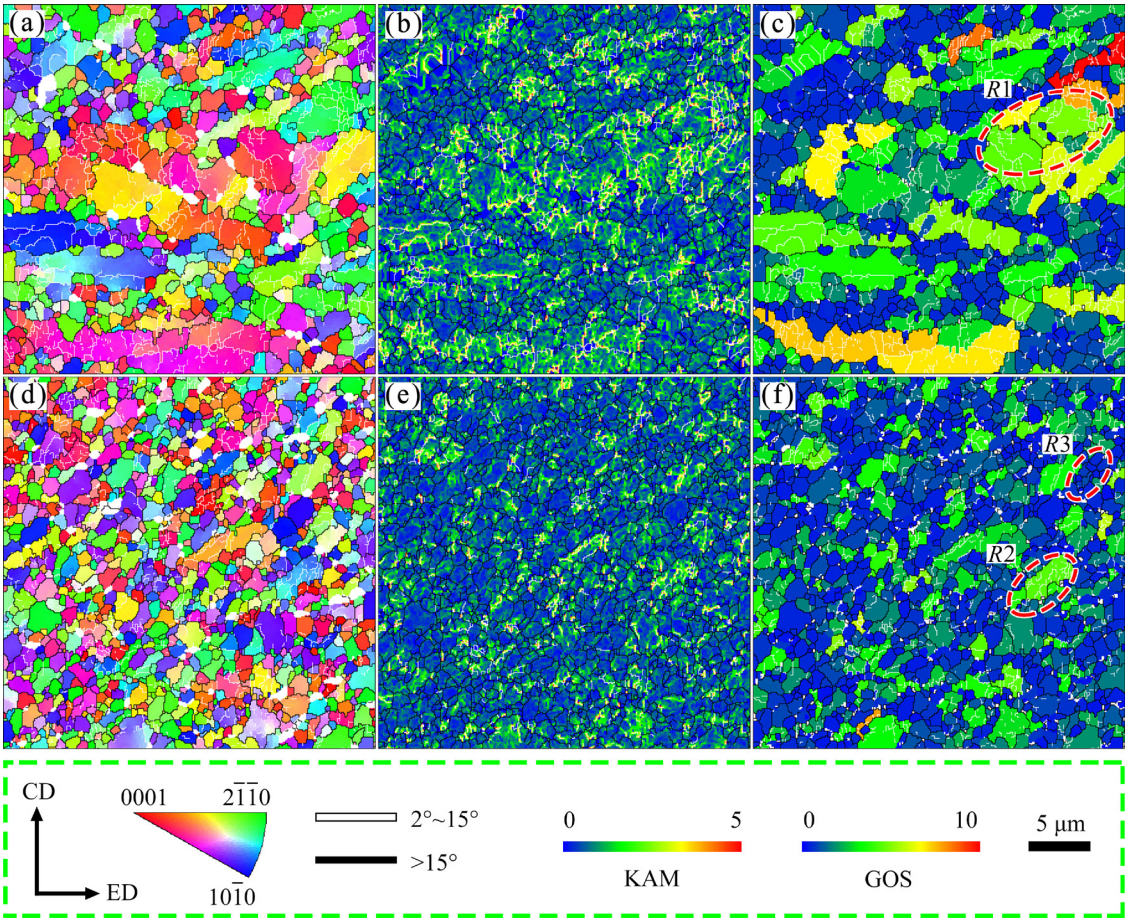

Fig. 5 IPF (a, d), KAM (b, e) and GOS (c, f) maps of different composites under thermal compression at 800 °C: (a−c) As-cast; (d−f) As-forged

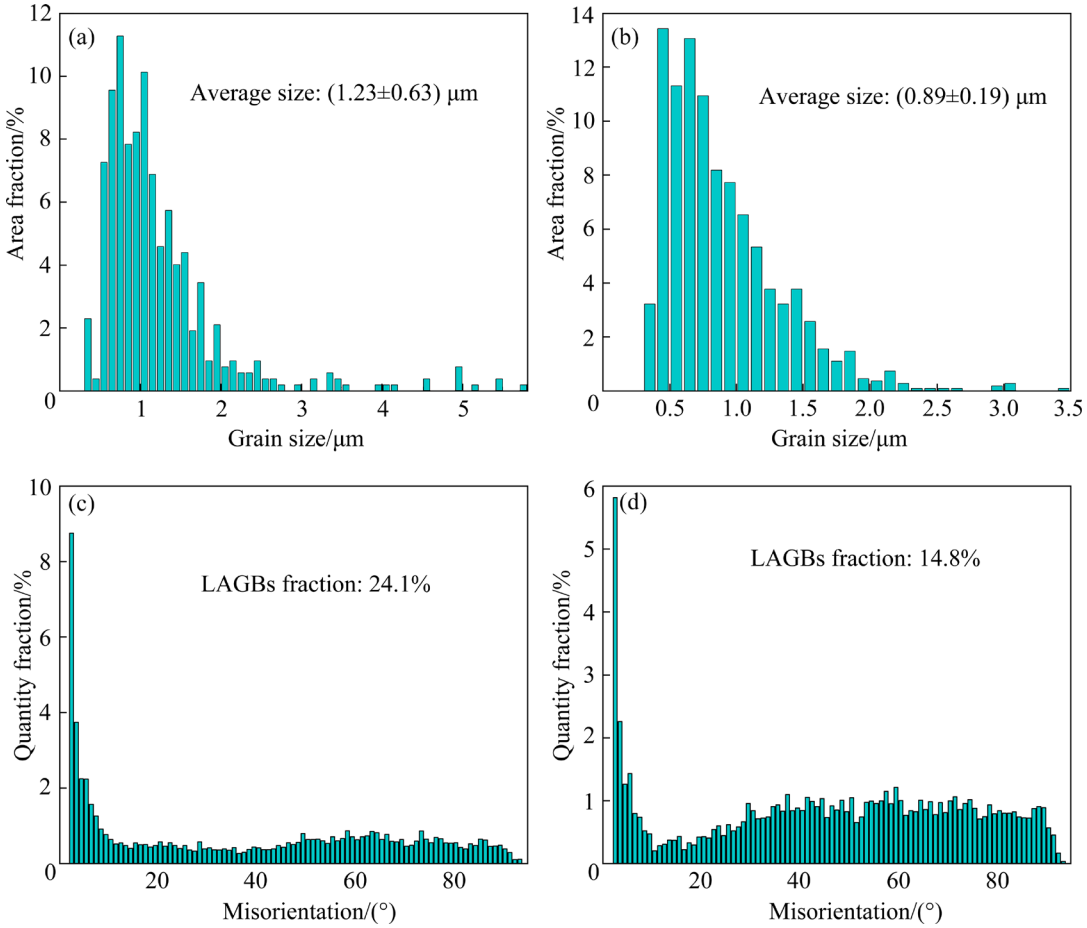

Fig. 6 Grain size (a, b) and misorientation angle distribution (c, d) of different composites under thermal compression at 800 °C: (a, c) As-cast; (b, d) As-forged

deformation resistance. The fine grains between these elongated grains should be DRXed grains which have low dislocation density. In contrast, most regions of Fig. 5(e) present a low strain state. The grain orientation spread (GOS) map expresses the average orientation change inside the grains. Generally, the orientation difference inside the DRXed grains is very small, hence it presents blue in the GOS map. The GOS maps of as-cast and as-forged composites are shown in the Figs. 5(c) and (f). According to statistics, the proportions of DRXed grains are 41.1% and 79.6%, respectively.

Figure 7 shows the GOS diagrams of three selected special areas of composite after thermal compression at 800 °C. Some new fine grains (labeled g1−g4) are formed along the edge of coarse deformed grains (labeled G1−G4), indicating that the formation of these new grains depends on the bulges of the HAGBs of the parent grains, which is closely related to the thermal deformation process. It can be seen that the grain boundaries of coarse grains have complex contour profiles. These serrated grain boundaries are easy to migrate under the action of stress, thus becoming the nucleation sites of DRX grains [25,26]. The newly formed grains grow by swallowing the surrounding grains. In addition, the interior of the coarse grains is divided into some sub-grains by LAGBs. The distribution of misorientation from point to origin along *AB* direction (Fig. 7(c)) shows that the misorientation will suddenly change when the line passes through the sub-grain boundaries. The cumulative misorientation from *A* to *B* reaches 17°, indicating that with the increase of strain, the sub-grain boundaries continue to accumulate dislocations, the misorientation with the parent grains continue to increase, and finally DRXed grains (labeled g5−g6) appear in the grains. From the crystal orientation distribution map (Fig. 7(b)), it is found that DRXed grains have random crystallographic orientation, but the orientation of each coarse deformed grain remains relatively

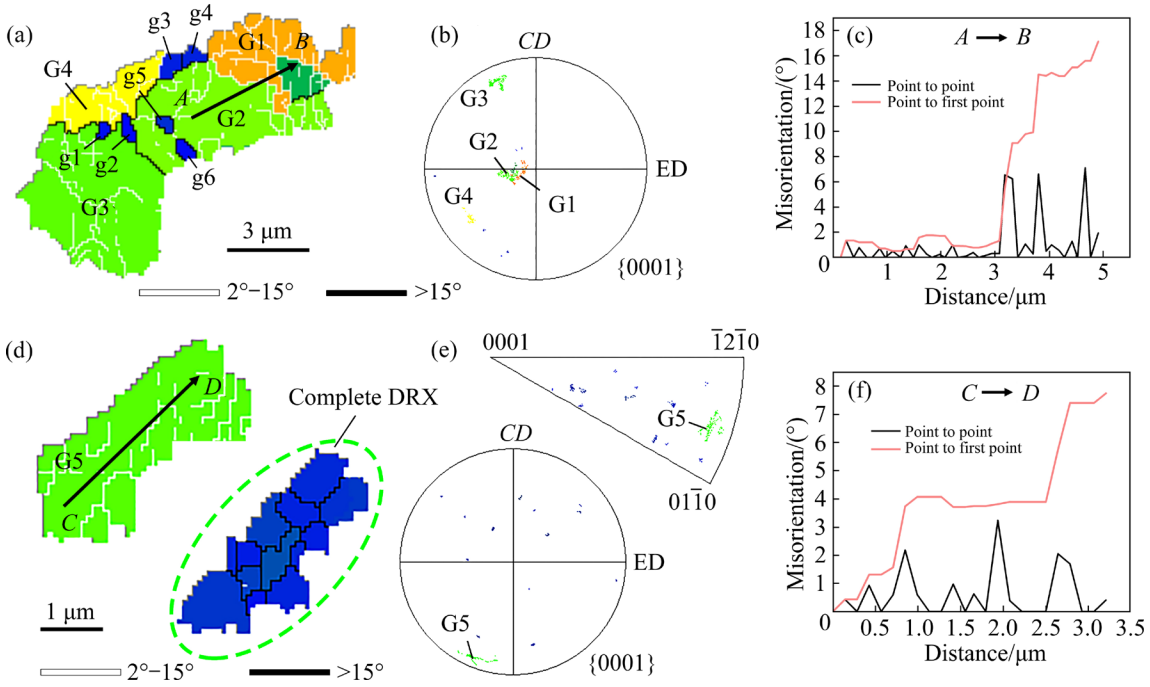

Fig. 7 DRX mechanism after thermal compression at 800 °C: (a, d) GOS maps of *R*1, *R*2 and *R*3 regions in Fig. 5 (G1−G5: Coarse unDRXed grains; g1−g6: DRXed grains); (b, e) Crystal orientation distribution of DRXed grains and substructures; (c, f) Misorientation diagrams along *AB* and *CD* direction

consistent. According to previous reports [20,27], g1−g4 grains can be classified as discontinuous dynamic recrystallization (DDRX) and g5−g6 grains can be sorted out as CDRX. Therefore, it can be concluded that DRX under this condition is a mechanism of DDRX and CDRX coupling. Figures 7(d−f) show the DRX mechanism of grains in *R*2 and *R*3 regions (Fig. 5) of as-forged composite after thermal compression at 800 °C. The cumulative misorientation of a single coarse grain along the *CD* direction is 8°, indicating that the grain does not accumulate enough dislocations, the rotation degree of sub-grains is relatively low, and DRX does not occur. Compared with the region with complete DRX at the lower right, it can be asserted that these DRXed grains are formed by the continuous crystal rotation of the sub-grains on both sides of the LAGBs and the gradual increase of the misorientation, in other words, the CDRX mechanism dominates the DRX process.

3.5 Roles of reinforcements on DRX

As mentioned above, the as-forged composite has more sufficient DRX in the process of thermal compression, and it has smaller grain size and more grain boundaries, which is conducive to the precipitation of silicides. Therefore, the forged samples are selected to study the precipitation behavior of silicide. The TEM micrographs (Figs. 8(a, b)) show that the matrix contains DRXed grains, substructures, dislocation cells and some ellipsoidal precipitates. The size of precipitates is in the range of 70−400 nm, and most of them are embedded in the grain boundaries or inside the grains. Based on the results of EDS and SAED (Figs. 8(c, d)), it is concluded that the precipitates are S2-type silicides. Some sub-grain boundaries divide large deformed grains into several cellular structures. In the subsequent deformation process, these cellular structures will become complete grains, which confirms that the DDRX mechanism plays a role under this condition. It is worth noting that most silicides appear at the end of the sub-grain boundaries and the area where dislocations gather, indicating that the silicides precipitated in advance during the hot deformation process hinder the movement of dislocations, resulting in the accumulation and entanglement of dislocations around them, and finally form the structures of sub-grain boundaries and dislocation cells. Moreover, the cross entangled dislocations will act as the diffusion channel of Si and Zr atoms, which

induces the secondary precipitation of silicides.

The synergistic effect of reinforcements on DRX is shown in Fig. 9. After pre-deformation, α lamellas are refined and partially bent, and dislocations gather around the reinforcements and grain boundaries (Fig. 9(a)). In the subsequent thermal compression period, TiB_w and Y_2O_3 particles do not coordinate with the deformation of the matrix, resulting in stress concentration, and dislocations further proliferate and gather in these areas, forming dislocation entanglement and some cellular structures (Fig. 9(b)). High-density dislocations provide energy for the subsequent DRX process and promote the refinement of local grains. Notably, the silicides precipitate preferentially along the grain boundaries and dislocations. Firstly, the silicides precipitated at grain boundaries can pin grain boundaries and inhibit the growth of fine grains. Secondly, the silicides precipitated from dislocations can hinder the slip of dislocations, resulting in the entanglement of dislocations. During further deformation, the accumulated dislocations will rearrange and annihilate to form dislocation walls and LAGBs, and generate some dislocation cells. With the continuation of deformation, the misorientation between adjacent sub-grains increases, and finally a coarse deformed grain is decomposed into some fine DRX grains (Fig. 9(c)), which is consistent with the research of MA et al [28]. Based on the above analysis, it can be concluded that the reinforcements and silicides precipitated at grain boundaries and dislocations synergistically promote the DRX of α phase. It is worth noting that due to the low deformation temperature (800 °C), the diffusion ability of elements decreases, and Si, Zr and other elements can only diffuse for a short distance, so that the growth process of silicides after nucleation is inhibited, and the final silicides are small in size and evenly distributed. Therefore, a reasonable adjustment of the thermal deformation temperature can control the fine, uniform and dispersed precipitation of silicides on the matrix, so as to improve the strength and plasticity of the alloy at the same time.

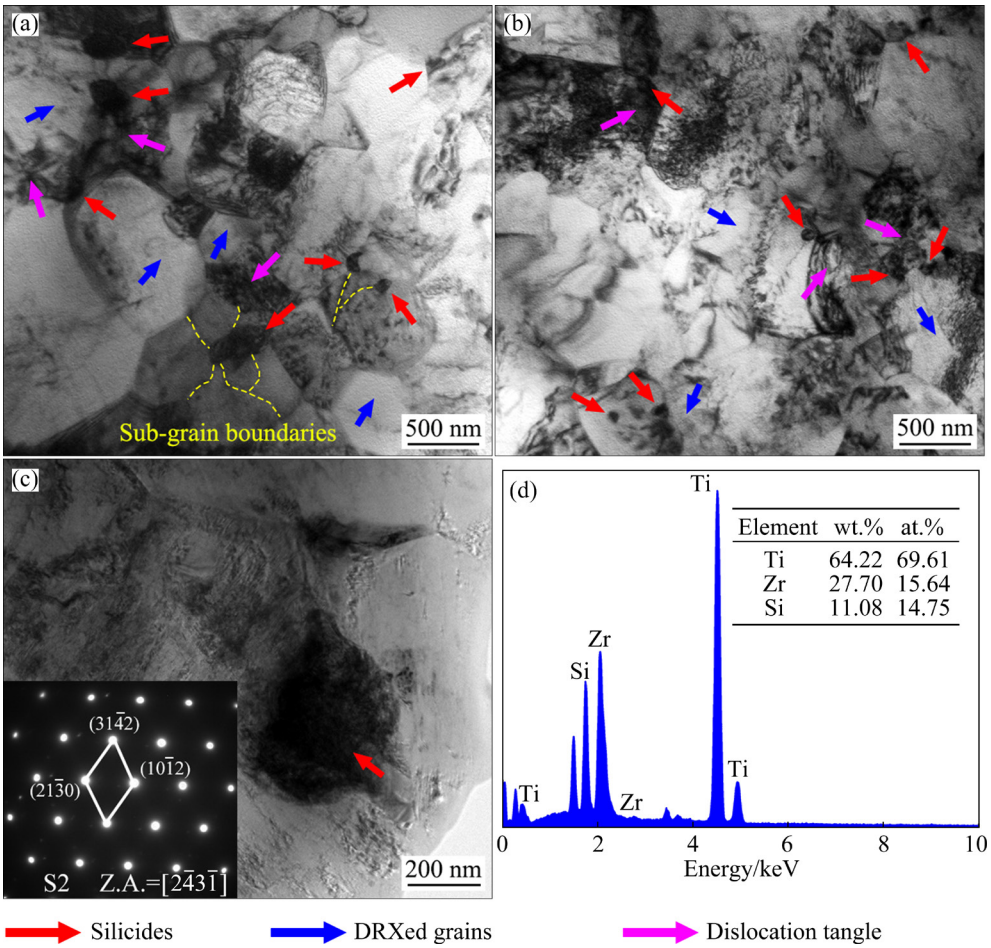

Fig. 8 Precipitation behavior of as-forged composite after thermal compression at 800 °C: (a, b) TEM image; (c) Morphology and SAED diagram corresponding to precipitation; (d) EDS result

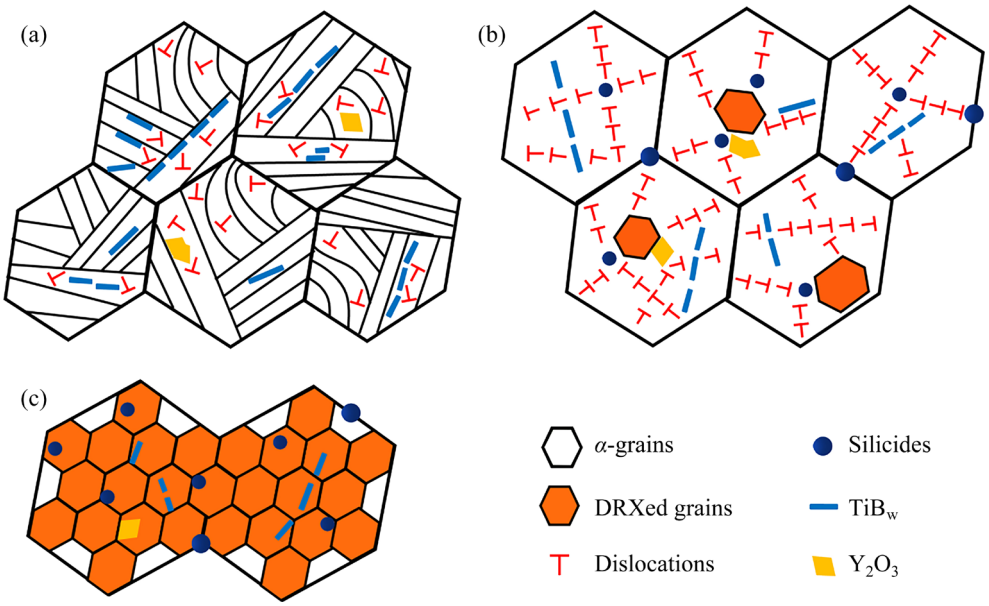

Fig. 9 Schematic diagram of synergistic effect of reinforcements and silicides on DRX during thermal compression at 800 °C: (a) Microstructure of composite after pre-deformation; (b) Generation of dislocation cells and LAGBs during hot compression; (c) Formation of ultrafine DRX grains

4 Conclusions

(1) With increasing temperatures, the size of silicide precipitated during compression continues to increase, while its quantity first increases and then decreases. The dislocations accumulated in the composite matrix during pre-deformation induce the transformation of the precipitation position of silicide from α/β interfaces or β blocks to uniformly inside the matrix.

(2) The proportions of DRX of as-cast and as-forged composites after hot compression at 800 °C are 41.1% and 79.6%, respectively. The pre-deformation transforms the grain refinement mechanism from CDRX and DDRX coupling to complete CDRX.

(3) During the hot compression deformation, high-density dislocations gather around the broken TiB_w and polymerized Y_2O_3 reinforcements due to stress concentration, which promotes the refinement of local grains. According to the precipitation position, the promoting effect of silicide on DRX of α grains can be attributed to pinning grain boundaries and hindering dislocation slip.

Acknowledgments

The authors are grateful for the financial supports from the National Natural Science Foundation of China (Nos. 52171122, 52071228, 51904205, 51901151), the Natural Science Foundation of Shanxi Province, China (No. 20210302124077), the Central Government Guides the Special Fund Projects of Local Scientific and Technological Development, China (No. YDZJSX2021A016), the Natural Science Foundation of Ningxia, China (No. 2022AAC02077), and the Key Research and Development Program of Shanxi Province, China (Nos. 201903D421084, 201903D121056).

References

[1] MORSI K. Review: Titanium–titanium boride composites [J]. Journal of Materials Science, 2019, 54(9): 6753−6771.

[2] HAYAT M D, SINGH H, HE Zhen, CAO Peng. Titanium metal matrix composites: An overview [J]. Composites Part A: Applied Science and Manufacturing, 2019, 121: 418−438.

[3] XU Li-juan, ZHENG Yun-fei, LIANG Zhen-quan, XUE Xiang, HAN Shi-wei, XIAO Shu-long, TIAN Jing, CHEN Yu-yong. Effect of stress and temperature on creep behavior of a (TiB + TiC + Y_2O_3)/ alpha-Ti composite [J]. Materials Characterization, 2021, 181: 111495.

[4] ZHANG C J, QU J P, WU J, ZHANG S Z, HAN J C, HAYAT M D, CAO P. A titanium composite with dual reinforcements of micrometer sized TiB and submicrometer sized Y_2O_3 [J]. Materials Letters, 2018, 233: 242−245.

[5] ZHAO Er-tuan, SUN Shi-chen, ZHANG Yu. Recent advances in silicon containing high temperature titanium

alloys [J]. Journal of Materials Research and Technology, 2021, 14(3): 3029−3042.

[6] WANJARA P, JAHAZI M, MONAJATI H, YUE S. Influence of thermomechanical processing on microstructural evolution in near-α alloy IMI834 [J]. Materials Science and Engineering A, 2006, 416(1/2): 300−311.

[7] CHANDRAVANSHI V K, SARKAR R, KAMAT S V, NANDY T K. Effect of boron on microstructure and mechanical properties of thermomechanically processed near alpha titanium alloy Ti-1100 [J]. Journal of Alloys and Compounds, 2011, 509(18): 5506−5514.

[8] CHEN Wei, ZENG Wei-dong, XU Jian-wei, ZHOU Da-di, WANG Si-min, HE Sheng-tong. Deformation behavior and microstructure evolution during hot working of Ti60 alloy with lamellar starting microstructure [J]. Journal of Alloys and Compounds, 2019, 792: 389−398.

[9] NIU Yong, LI Miao-quan. Effect of 0.16 wt.% hydrogen addition on high temperature deformation behavior of the Ti600 titanium alloy [J]. Materials Science and Engineering A, 2009, 513/514: 228−232.

[10] SHIMAGAMI K, ITO T, TODA Y, YUMOTO A, YAMABE-MITARAI Y. Effects of Zr and Si addition on high-temperature mechanical properties and microstructure in Ti−10Al−2Nb-based alloys [J]. Materials Science and Engineering A, 2019, 756: 46−53.

[11] ZHAO Y Q, QU H L, ZHU K Y, WU H, LIU C L, ZHOU L. The second phases in Ti40 burn resistant alloy after high temperature exposure for a long time [J]. Journal of Alloys and Compounds, 2002, 333(1/2): 165−169.

[12] JIAO Y, HUANG L J, WEI S L, PENG H X, AN Q, JIANG S, GENG L. Constructing two-scale network microstructure with nano-Ti_5Si_3 for superhigh creep resistance [J]. Journal of Materials Science & Technology, 2019, 35(8): 1532−1542.

[13] SINGH A K, RAMACHANDRA C. Characterization of silicides in high-temperature titanium alloys [J]. Journal of Materials Science, 1997, 32(1): 229−234.

[14] RAMACHANDRA C, SINGH A K, SARMA G M K. Microstructural characterisation of near-α titanium alloy Ti−6Al−4Sn−4Zr−0.70Nb−0.50Mo−0.40Si [J]. Metallurgical & Materials Transactions A, 1993, 24(6): 1273−1280.

[15] JIA Wei-ju, ZENG Wei-dong, YU Han-qing. Effect of aging on the tensile properties and microstructures of a near-alpha titanium alloy [J]. Materials & Design, 2014, 58(6): 108−115.

[16] JIAO Y, HUANG L J, GENG L, LI X T, GAO Y N, QIAN M F, ZHANG R. Nano-scaled Ti_5Si_3 evolution and strength enhancement of titanium matrix composites with two-scale architecture via heat treatment [J]. Materials Science and Engineering A, 2017, 701: 359−369.

[17] SUN Shi-chen, ZHAO Er-tuan, HU Chen, AN Yu-kun, CHEN Wen-zhen. Precipitation behavior of silicide and synergetic strengthening mechanisms in TiB-reinforced high-temperature titanium matrix composites during multi-directional forging [J]. Journal of Alloys and Compounds, 2021, 867: 159051.

[18] SU Yu, KONG Fan-tao, YOU Feng-hai, WANG Xiao-peng, CHEN Yu-yong. The high-temperature deformation behavior of a novel near-α titanium alloy and hot-forging based on the processing map [J]. Vacuum, 2020, 173:109135.

[19] ZHAO Er-tuan, SUN Shi-chen, YU Jin-rui, AN Yu-kun, CHEN Wen-zhen, SHEN Rui-run. Dynamic recrystallization and silicide precipitation behavior of titanium matrix composites under different strains [J]. Transactions of Nonferrous Metals Society of China, 2021, 31(11): 3416−3427.

[20] SUN Yong-gang, ZHANG Chang-jiang, FENG Hong, ZHANG Shu-zhi, HAN Jing-chao, ZHANG Wang-gang, ZHAO Er-tuan, WANG Hong-wei. Dynamic recrystallization mechanism and improved mechanical properties of a near α high temperature titanium alloy processed by severe plastic deformation [J]. Materials Characterization, 2020, 163: 110281.

[21] SUN Yong-gang, ZHANG Chang-jiang, JI Xiang, ZHANG Shu-zhi, FENG Hong, HOU Zhao-ping, HAN Fu-yin. Microstructure evolution of TiB_w/Ti composites during severe plastic deformation: Spheroidization behavior [J]. Materials Characterization, 2021, 171: 110725.

[22] CHEN Run, AN Qi, ZHANG Rui, LIU Yue, WANG Shuai, HUANG Lu-jun, GENG Lin. Effects of hot rolling on the microstructure and mechanical properties of network structured (TiB_w+$(TiZr)_5Si_3$)/TA15 composites [J]. Journal of Netshape Forming Engineering, 2021, 13(3): 1−8.

[23] LI Yang, CHEN Yue, LIU Jian-rong, HU Qing-miao, YANG Rui. Cooperative effect of silicon and other alloying elements on creep resistance of titanium alloys: Insight from first-principles calculations [J]. Scientific Reports, 2016, 6: 30611.

[24] SOUZA P M, HODGSON P D, ROLFE B, SINGH R P, BELADI H. Effect of initial microstructure and beta phase evolution on dynamic recrystallization behaviour of Ti6Al4V alloy—An EBSD based investigation [J]. Journal of Alloys and Compounds, 2019, 793: 467−479.

[25] LIU Zhang-guang, LI Pei-jie, XIONG Liang-tong, LIU Tai-ying, HE Liang-ju. High-temperature tensile deformation behavior and microstructure evolution of Ti55 titanium alloy [J]. Materials Science and Engineering A, 2017, 680: 259−269.

[26] WANG Ke, WU Ming-yu, REN Zhao, ZHANG Yu, XIN Ren-long, LIU Qing. Static globularization and grain morphology evolution of α and β phases during annealing of hot-rolled TC21 titanium alloy [J]. Transactions of Nonferrous Metals Society of China, 2021, 31(9): 2664−2676.

[27] JIANG M G, XU C, YAN H, FAN G H, NAKATA T, LAO C S, CHEN R S, KAMADO S, HAN E H, LU B H. Unveiling the formation of basal texture variations based on twinning and dynamic recrystallization in AZ31 magnesium alloy during extrusion [J]. Acta Materialia, 2018, 157: 53−71.

[28] MA X Z, XIANG Z L, MA M Z, CUI Y P, REN W M, WANG Z T, HUANG J C, CHEN Z Y. Investigation of microstructures, textures, mechanical properties and fracture behaviors of a newly developed near α titanium alloy [J]. Materials Science and Engineering A, 2020, 775: 138996.

热变形温度和预变形对(TiB+Y_2O_3)/近α钛基复合材料硅化物析出行为的影响

连启豪[1]，张长江[1,2,3]，冯 弘[1]，杨振博[1]，张树志[1]，韩建超[2]，王 涛[2]，彭 凡[3]，曹 鹏[4]

1. 太原理工大学 材料科学与工程学院，太原 030024；
2. 教育部先进金属复合材料成形技术与设备工程研究中心，太原 030024；
3. 共享装备股份有限公司，银川 750021；
4. Department of Chemical and Materials Engineering, University of Auckland, New Zealand

摘 要：基于热压缩试验，研究变形温度和预变形对(TiB+Y_2O_3)双增强相近 α 钛基复合材料显微组织演变的影响。结果表明：热变形时析出的硅化物的尺寸随变形温度的升高而增大，但其析出数量呈先增加后减少的趋势。预变形使硅化物的析出位置由 α/β 界面或 β 块扩散到整个基体组织。动态再结晶是复合材料晶粒细化的主要原因，由预变形引入的位错加速连续动态再结晶的进程。在变形时，位错在断裂的 TiB_w 和富集的 Y_2O_3 增强相周围大量增殖和聚集，推动局部晶粒的细化。不同于 TiB_w 和 Y_2O_3 对晶粒细化的影响，根据其分布位置的不同，纳米硅化物分别通过钉扎晶界和阻碍位错运动促进 α 晶粒的动态再结晶。

关键词：近 α 钛基复合材料；显微组织演变；硅化物析出；动态再结晶；热压缩变形

(Edited by Xiang-qun LI)